

Aminosilane Modified Clay Nanotubes as a Template for Visible Light Active Ru/CdS Photocatalysts

F. Pouresmaeil^a, A. Kurenkova^b, A. Stavitskaya^{a,*}, D. Kopitsyn^a, E. Kozlova^{b,c},
E. Ivanov^a, P. Gushchin^a, and V. Vinokurov^a

^a Gubkin University, Moscow, 119991 Russia

^b Boreskov Institute of Catalysis SB RAS, Novosibirsk, 630090 Russia

^c Novosibirsk State University, Novosibirsk, 630090 Russia

*e-mail: stavitsko@mail.ru

Received September 23, 2020; revised December 8, 2020; accepted December 24, 2020

Abstract—The aminosilane modified natural halloysite nanotubes were efficiently used as a template for ruthenium doped cadmium sulfide nanoparticles to prevent particles agglomeration and increase photocatalytic activity via better electron-hole pair separation. The photocatalysts were synthesized via a facile method and tested in H₂ evolution reaction under visible light irradiation with 0.1 mol L⁻¹ Na₂S and 0.1 mol L⁻¹ Na₂SO₃ as sacrificial agents. The as-prepared samples were characterized by transition electron microscopy, thermo-gravimetric analysis, photoluminescence spectrometry. The Ru–CdS nanoparticles synthesized on amino-modified halloysite nanotubes (Ru–CdS/Hall-APTES) had a high photocatalytic H₂ evolution rate of 932.3 μmol h⁻¹ g⁻¹ and apparent quantum efficiency (AQE) about 7.2% under monochromatic 450 nm light irradiation. The well-enhanced photocatalytic activity of Ru–CdS/Hall-APTES composite could be attributed to the effective transfer and separation of photogenerated charge carriers, which is facilitated by Ru as a co-catalyst to assist photocatalytic H₂ evolution reaction. This work seems to provide an approach to prepare high-performance halloysite based nanocomposites towards different applications, like the as-studied photocatalytic production of hydrogen.

DOI: 10.1134/S2635167621020129

INTRODUCTION

Cadmium sulfide is a widely studied semiconductor with a band gap of 2.42 eV. It has a proper VB and CB position which makes it capable of driving both reduction and oxidation of water under visible light irradiation [1, 2]. It can be used as a promising photocatalyst; however some negative points like toxicity and fast recombination of photoexcited charge carriers, hinders its application [3]. From the photocatalytic point of view, it can be admitted that the most important drawback of cadmium sulfide is its instability while the photoexcited charge carriers are recombined fast and due to its oxidation during the photocatalytic reaction, photocorrosion is occurred [4]. Thus, finding solutions to improve the stability of CdS nanoparticles has become an issue for many studies. Combining with other semiconductors [5, 6], doping with other elements [7–9] and synthesis of various morphological CdS structures [10, 11] are some of the implemented works to the date.

One of the approaches to prevent agglomeration of nanoparticles is using other materials as a support [4, 12]. Thus, it improves the stability and besides, increases the surface area. Recently tubular mineral

clays of halloysite were studied as support for settling different nanomaterials on its surface [13–15]. These nanotube-shaped clay minerals have lately attracted interests, due to their unique properties in comparison with widely used expensive carbon nanotubes. It is easy to imagine that soon halloysite nanotubes (HNTs) could replace the much more expensive carbon nanotubes, and in many cases, HNTs could be used in high technological applications where carbon nanotubes are just not suitable [14].

However, application of halloysite is currently limited by its highly hydrophilic internal and external surfaces, due to the presence of polar groups, according to which the chemical functionalization of HNTs is required.

The aluminols (Al–OH) are primarily located in the lumen of the HNTs, while the outer surface is filled with siloxanes (Si–O), and at the edges of the layers, there are a few silanols (Si–OH) and aluminols (Al–OH) [16]. These hydroxyl groups are the potential reactive sites for the surface modification on the external surface of halloysite nanotubes, which increases the interaction of the functionalizing agent with halloysite nanotubes [17].

Importantly, the effective modification depends strongly on the structure of the organosilane, considering the size and functional group and the reaction conditions [18].

Halloysite functionalization with (3-aminopropyl)triethoxysilane (APTES) is of high interest in recent studies [16, 17, 19–21]. The APTES-functionalized HNTs showed the highest silylation efficiency [16]. The silylation reaction occurred at Al–OH groups of the inner lumen surface and the edges as well as Si–OH groups at the edges of external surface defects [16].

The cocatalysts loaded on semiconductor photocatalysts play an essential role in the production of H₂ and O₂ and can greatly enhance the activities of photocatalysts. During the electron-hole separation, the excited holes are accumulated on the surface exhibiting high oxygen evolution activity in the oxidation half-reaction, while the electrons prefer to stay at the bulk of semiconductor. The role of a co-catalyst here is to take the photogenerated electrons to the surface of the catalyst [22–24]. The assumed mechanism for this reaction is discussed in different studies [22, 23]. Ru seems to be a more active co-catalyst than Pt while in [25] Ru–EY photocatalyst showed 4.9 times higher hydrogen generation activity than Pt–EY under the same conditions.

In this study, we aimed to synthesize a halloysite-based photocatalyst with an effective photocatalytic activity under visible light. In order to achieve that goal, halloysite inner and outer surface was firstly modified with (3-aminopropyl) triethoxysilane, so that the surface was fully covered with amine functional groups. Then, we grafted CdS nanoparticles on it via a facile method, and we promoted the photocatalytic activity by adding Ru as a co-catalyst. We have provided a facile method for the synthesis of a clay-based photocatalyst with a relatively excellent photocatalytic activity; however there still remains a requirement to more cost-effective photocatalysts by not using precious metals as cocatalysts.

EXPERIMENTAL

Materials

Halloysite was purchased from the Zhengzhou Jinyang Guang Chinaware Co., Ltd., Henan, China and used as received. (3-Aminopropyl)triethoxysilane (APTES), cadmium nitrate tetrahydrate (Cd(NO₃)₂ · 4H₂O), thioacetamide (C₂H₅NS), ethanol 96% (C₂H₅OH), ruthenium(III) chloride RuCl₃ (45–55% Ru content) were all purchased from Sigma-Aldrich. Toluene (99.5%), ammonium hydroxide (NH₄OH) (0.9 g/cm³) were received from the Ecos Co., Moscow, Russia. All reagents were in analytical grade and used without further purification.

Halloysite Surface Modification with (3-Aminopropyl)triethoxysilane

Halloysite inner and outer surface were modified with APTES. The process was carried out according to a literature method [17]. For modification, 6 g of halloysite was dispersed in dry toluene. A solution of 1.5 mL APTES in 25 mL toluene was added. The mixture was then refluxed at 120°C for 6 h, and then it was washed extensively with toluene for three times to remove the excess of APTES and was dried overnight at 70°C for further curing. It is shown in Fig 1.

Preparation of Ru/CdS-Hall-APTES

At the initial stage, CdS/Hall-APTES was prepared. Synthesizing CdS on the surface of the as-prepared modified halloysite (Hall-APTES) was as follows: a solution of 0.1 g Cd(NO₃)₂ · 4H₂O in ethanol (10 mL) was added to a dispersion of 0.5 g modified clay in 15 mL of ethanol and was ultrasonicated for 30 min. Then a solution of thioacetamide (TAA) corresponding to the amount of Cd, in order to have a ratio of Cd/S = 1, was added to the mixture under continuous mixing. Finally, 1 mL of ammonium hydroxide (NH₄OH) was added to keep pH in the basic limit. The color of the solution in this step was bold yellow. The final solution was centrifuged and washed for three times and dried at 70°C.

At the second stage, Ru–CdS/Hall-APTES was prepared as follows: an ethanol solution of 2.5 mg RuCl₃ (0.0004 g/mL) was added dropwise to 0.1 g of CdS/Hall-APTES, dispersed in ethanol.

The color in this stage changed to dark green. The solution was ultrasounded for 30 min, washed with ethanol for three times and dried at 60°C. Figure 1 shows the preparation of Ru–CdS/Hall-APTES, while in Fig. 2, the chemical change of halloysite's surface in each stage is presented.

Material Characterization

The apparent and internal morphologies were conducted by Transmission Electron Microscopy (TEM) using a JEM-2100 transmission electron microscope (Jeol, Tokyo, Japan). Thermogravimetric analyses (TGA) were carried out using a Universal V4.5A TA instrument. The samples were heated from 30 to 950°C at a heating rate of 5°C min⁻¹ under nitrogen flow. The photoluminescence (PL) spectra were measured using a fluorometer (Agilent Cary Eclipse) at room temperature. Elemental analysis was performed on an ARL Quant'X energy-dispersive spectrometer (Thermo Fisher Scientific, Waltham, MS, USA) in air. The results were processed using the standard-less UniQuant method.

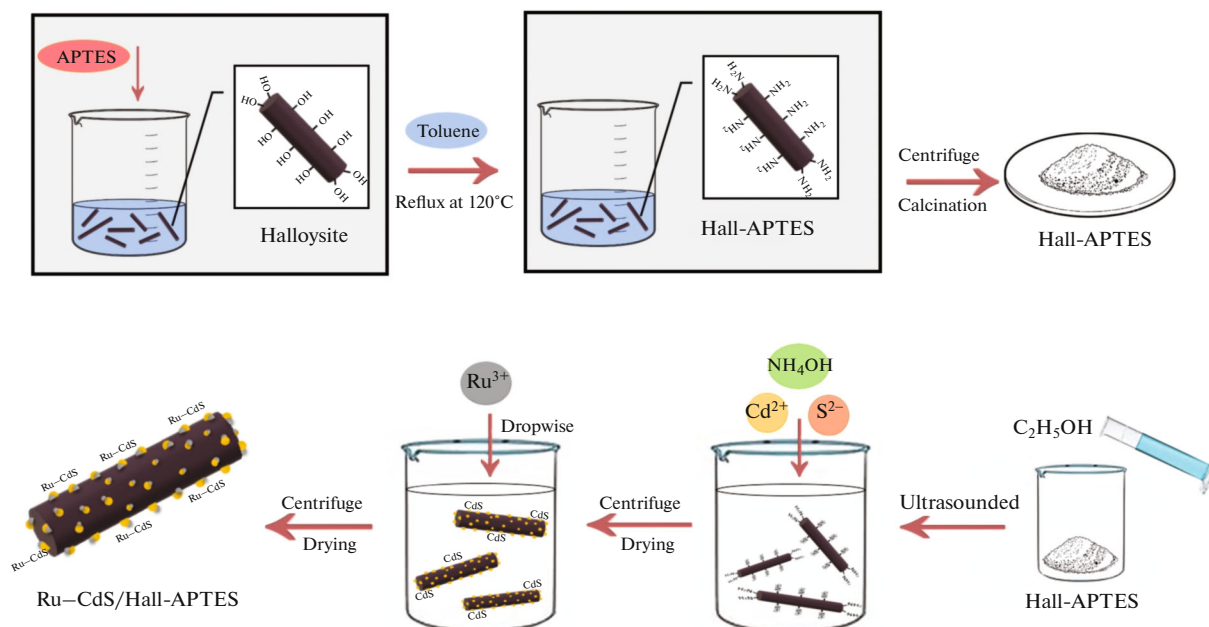


Fig. 1. (Color online) Preparation of Ru–CdS/Hall-APTES.

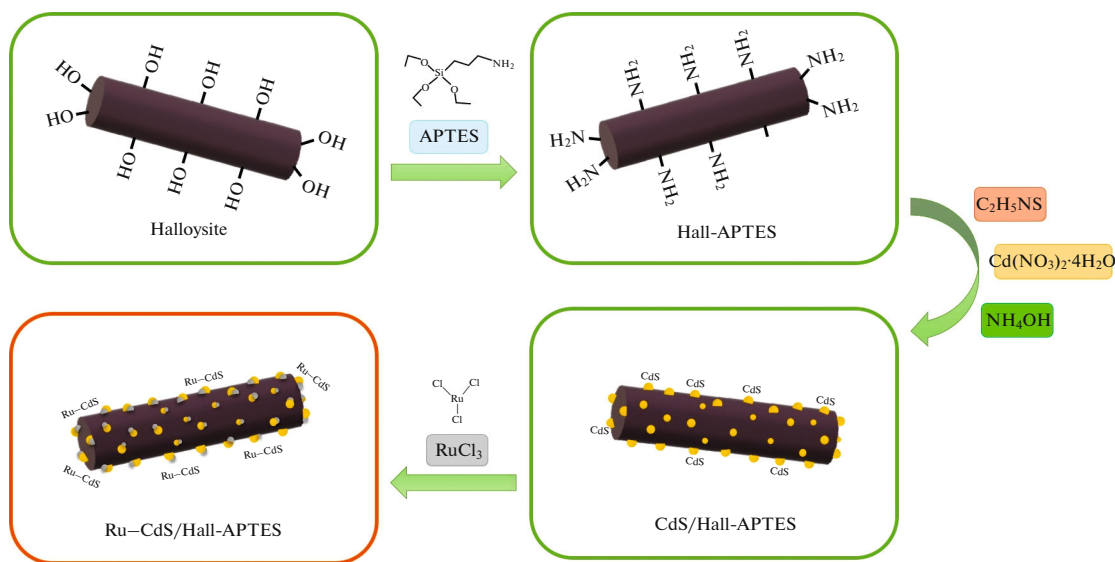


Fig. 2. (Color online) The assumed chemical change of halloysite's surface.

Measurement of Photocatalytic Activity

In a typical photocatalytic reaction, 50 mg powder of the sample was dispersed in an aqueous solution (100 mL) containing 0.1 M Na_2S and 0.1 M Na_2SO_3 . The mixture was ultrasonicated for 10 min and then bubbled with argon gas for 20 min to remove the dissolved oxygen. Afterward, the suspension was sealed and placed into a thermostated reactor and was irradiated with a 450 nm LED (30 W, China, 40 mV/cm^2).

The gases evolved, wherein the concentration of hydrogen gas was analyzed in line with a gas chro-

matograph (LChM-8 (Russia), TCD, with a zeolite column and Ar as the carrier gas). The apparent quantum yield (AQY) was calculated according to the following equations:

$$\text{AQY}(\%) = \frac{\text{Number of reacted electrons}}{\text{Number of incident photons}} \times 100,$$

$$= \frac{\text{Number of evolved } \text{H}_2 \text{ molecules} \times 2}{\text{Number of incident photons}} \times 100.$$

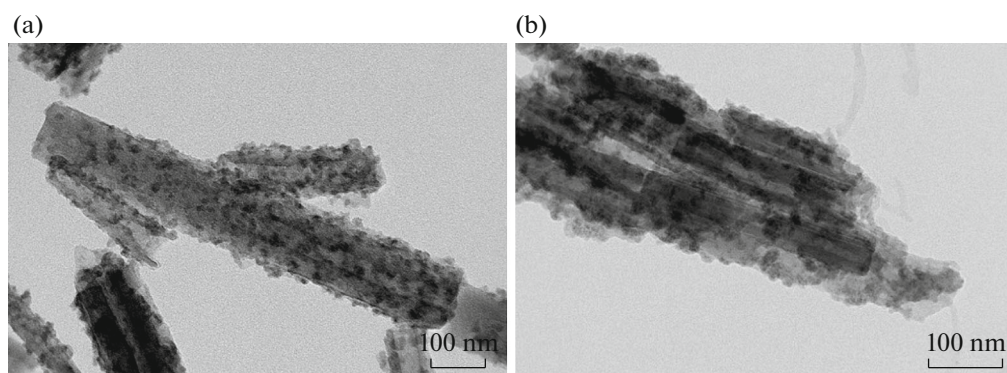


Fig. 3. TEM images of CdS/Hall-APTES (a) and Ru-CdS/Hall-APTES (b).

As the calculated photon flux was $28 \mu\text{Ein-stein min}^{-1}$, therefore AQE at the wavelength of 450 nm can be calculated from the formula $\text{AQE}(\%) = (2W/28) \times 100\%$, where W is the rate of hydrogen formation in $\mu\text{mol/min}$ [26].

RESULTS AND DISCUSSION

Structural and Morphological Characterization

The TEM images showed that nanoparticles of CdS were grafted on Hall-APTES surface almost homogeneously, before and after adding Ru as a cocatalyst. Figures 3a, 3b show TEM images of CdS/Hall-APTES and Ru-CdS/Hall-APTES, respectively. As shown in Figs. 3a, 3b, nanoparticles of CdS are nearly dispersed homogeneously on the surface of HNTs. Elemental analysis showed that Ru-CdS/Hall-APTES contains 0.5 wt % of Ru and 10.5 wt % of Cd, which is correspondent to 13.6 wt % of CdS assuming Cd/S ratio of one.

According to the data from 200 times size measurement of nanoparticles from a range of TEM images of the samples, using ImageJ software, nanoparticles of CdS are ranged from 4–11 nm, and the average size was 6.9 nm. Figure 4 shows the size distribution of the nanoparticles due to their frequency.

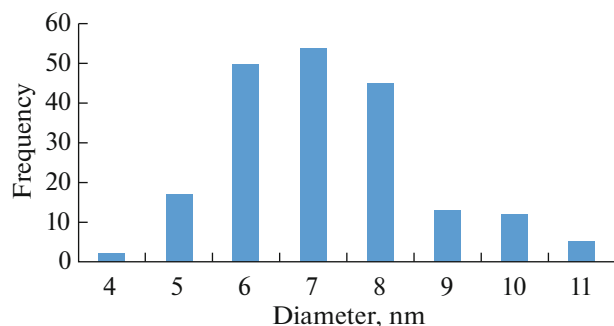


Fig. 4. (Color online) The size distribution of CdS nanoparticles in CdS/Hall-APTES.

Thermal Behavior

The thermal stability of the samples was evaluated through the TGA. Figure 5 shows the TGA-DSC plots of nanocomposites of organosilane-modified HNT with CdS and Ru-CdS. The thermal stability of materials can be associated with the inherent characteristics and the molecular interactions of samples [27]. There are mainly two major weight loss stages in thermograms, from 350 to 550 and from 570 to 870°C. The first major weight loss in the range from 350 to 550°C (13.8% for Ru-CdS/Hall-APTES and 13.9% for the sample without Ru), is associated with the dehydroxylation of structural Al-OH groups, present in HNTs and is accompanied by silane degradation [28]. In this range for the composite samples, two endothermic peaks are observed in 490 and 530°C, indicating the degradation of silane grafted onto HNTs surface and halloysite dihydroxylation process, respectively (Fig. 5). By increasing temperature from 550 to 870°C, the second significant weight losses of CdS/Hall-APTES (13.9%) and Ru-CdS/Hall-APTES (14.4%) are observed indicating mostly the CdS nanoparticles destruction. The degradation of halloysite also makes contribution to weight loss of the materials in this temperature range [28].

Optical Properties

The optical properties of CdS/Hall-APTES and Ru-CdS/Hall-APTES at room temperature were studied. Photoluminescence emission spectra of CdS/Hall-APTES samples before and after adding Ru, was recorded at an excitation wavelength of 350 nm. It is known that PL spectra are used to investigate the recombination of photogenerated charge carriers and to measure the efficiency of the separation of electron-hole pairs and therefore the charge transfer [29]. The lower the intensity of PL, the lower the charge recombination rate, and therefore the higher the photocatalytic activity of semiconductor photocatalysts. As can be seen in Fig. 6, the main broad emission peak for pure CdS/Hall-APTES and

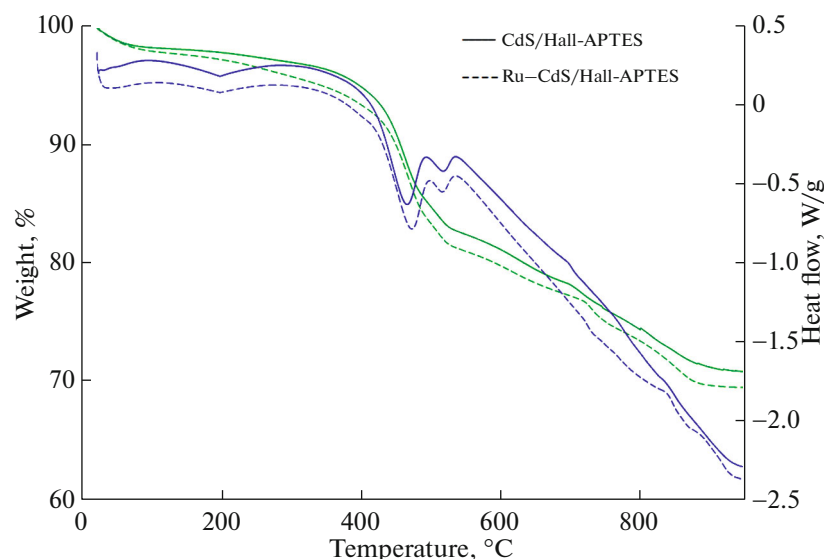


Fig. 5. (Color online) TGA-DSC curves for CdS/Hall-APTES and Ru-CdS/Hall-APTES.

Ru-CdS/Hall-APTES are almost the same and is centered at 425 nm. This represents the fact, that the loading of ruthenium as a co-catalyst has not induced new photoluminescence. Whereas, the peak intensity of Ru-CdS/Hall-APTES was lower than that of CdS/Hall-APTES, which indicates that the recombination of the electron-hole pairs was inhibited by adding Ru by rapid electron transfer to its atoms.

Photocatalytic activity. The Ru-CdS/Hall-APTES indicated an effective hydrogen production rate ($932.31 \mu\text{mol h}^{-1} \text{g}^{-1}$) in comparison with the sample CdS/Hall-APTES, which showed much lower photocatalytic activity values ($120 \mu\text{mol h}^{-1} \text{g}^{-1}$). The improve in photocatalytic activity could be attributed to the effective transfer and separation of photogenerated charge carriers by adding Ru as a co-catalyst, which is due to the decreased rate of electron-hole recombination. No appreciable H_2 evolution in the absence of either irradiation or a photocatalyst was detected in blank experiments, indicating that H_2 was produced via photocatalytic reactions.

Adding Ru as a co-catalyst increased the rate about 8 times, which implies that using Ru as a co-catalyst plays an important role in the photocatalytic activity towards hydrogen production.

For further comparison, the recently reported results in the field of photocatalysts on the base of CdS, have been summarized in Table 1. As observed in the table, although the H_2 -evolution activity of Ru-CdS/Hall-APTES in this study is smaller than that of some reports, but it is enough to prove that the Ru-CdS/Hall-APTES nanostructures hold great application potential in photocatalytic H_2 evolution.

Reaction Mechanism of Modification of Halloysite Nanotube with APTES

The mechanism of charge carrier separation is an important issue while investigating the process of semiconductor photocatalytic hydrogen evolution. When light is irradiated to the photocatalyst, herein Ru-CdS/Hall-APTES, electrons move from the valence band of the photocatalyst to the conduction band, leaving behind a hole with a positive charge in the VB (h_{VB}^+) and an electron in the CB (e_{CB}^-) (Eq. (1)). The photon should have an energy equal to or more than the bandgap energy of the semiconductor, in order to be able to perform charge separation [41].

Ru as a cocatalyst can inject the photo-generated electrons into the conduction band of CdS, under visible light illumination; meanwhile, the holes are accumulated on the surface. The electrons are trapped by

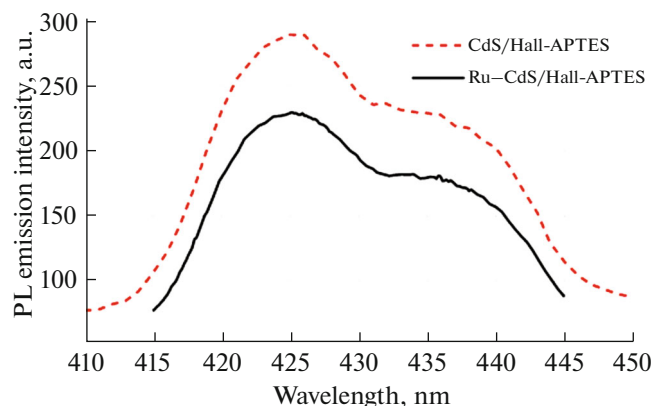


Fig. 6. (Color online) PL spectra of CdS/Hall-APTES (a) and Ru-CdS/Hall-APTES (b).

Table 1. Comparison of photocatalytic activity in hydrogen production of Ru–CdS/Hall-APTES and recently reported CdS-based photocatalysts

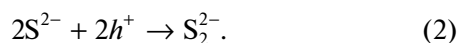
No.	Sample	Synthesis method	Co-catalyst	Light source	Activity ($\mu\text{mol h}^{-1} \text{g}^{-1}$)	Sacrificial reagent ($\text{S}^{2-}/\text{SO}_3^{2-}$) (M)	AQE %	Ref. (year)
1	Ru–CdS/Hall- APTES	Co-precipitation	0.5 wt % Ru	30 W 450 nm LED	932.31	0.1/0.1	7.21	This work
2	CdS NRs	Solvothermal/hydrothermal	3 mol % Co_3O_4	300 W Xe-lamp, $\lambda \geq 420$ nm	236	0.5/0.5		[30] (2015)
3	CdS NRs		8.4 mol % Co–Pi	$\lambda \geq 420$ nm	13 300	Lactic acid	24.3	[31] (2016)
4	g- C_3N_4 /CdS 1 wt %	Self-transformation method	1 wt % g- C_3N_4	$\lambda \geq 420$ nm	5303	0.35/0.25	3.61	[32] (2015)
5	CdS@ MoS_2 NWs	Hydrothermal	2 wt % MoS_2	300 W Xe lamp $\lambda \geq 420$ nm	493.1	Lactic acid	28.5	[33] (2017)
6	CdS NSs	Ultrasonic	1% MoS_2 NSs	300 W Xe-lamp, $\lambda \geq 420$ nm	1750	Lactic acid		[34] (2017)
7	Ni_2P @CdS	Solvothermal		$\lambda \geq 420$ nm	836.67		3.89	[35] (2018)
8	CSs/CdS 1%	Co-precipitation combined ageing method		300 W Xe-lamp, $\lambda \geq 420$ nm	583	0.5/0.5		[36] (2017)
9	CdS NPs/ CeO_2 NRs	Hydrothermal		300 W Xe-lamp, $\lambda \geq 420$ nm	8400	Lactic acid	11.2	[37] (2016)
10	CdS microcubes	Microwave-assisted hydrothermal		300 W Xe-lamp, $\lambda \geq 420$ nm	3051.4		4.9	[38] (2017)
11	Ti(IV)/CdS		TiO_2	350 W Xe-lamp, $\lambda \geq 420$ nm	2270.41	0.35/0.25		[39] (2016)
12	15% CdS/PI	Solvothermal method		$\lambda \geq 420$ nm	613	Lactic acid		[40] (2020)

the Ru nanoparticles which can effectively avoid charge recombination, while providing proton reduction sites for catalysis, therefore enabling excellent photocatalytic performance.

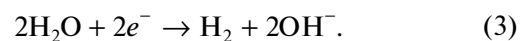
As shown in Fig. 7, the suggested assumed reactions are as follows:



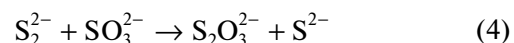
Photogenerated holes (h_{VB}^+) oxidize S^{2-} ions to water-soluble disulfide ion S_2^{2-} according to the equation [42]:



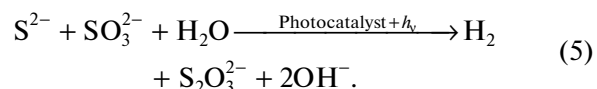
In this case, the photogenerated electrons from the CB reduce water by producing hydrogen:



In the presence of sulfite anions SO_3^{2-} in the solution, the following reaction occurs in the system:



with the formation of a water-soluble and uncolored disulfide anion. The overall reaction for H_2 evolution can be described by the equation [42]:



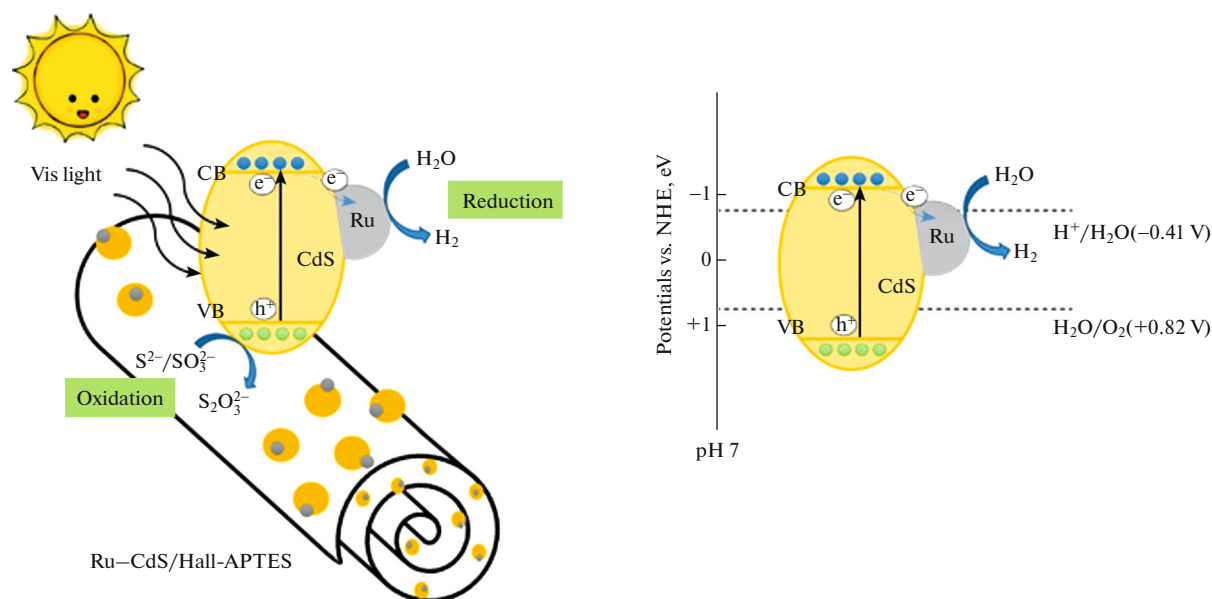


Fig. 7. (Color online) The proposed photocatalytic mechanism of Ru–CdS/Hall-APTES towards H₂ evolution.

CONCLUSION

In summary, the Ru–CdS/Hall-APTES composite was successfully synthesized by a facile strategy and applied into photocatalytic H₂ evolution in the presence of Na₂S and Na₂SO₃ solution as sacrificial reagents. Photocatalytic activity of Ru–CdS/Hall-APTES composite was remarkably enhanced by loading 0.5 wt % of Ru on the surface of CdS/Hall-APTES. The promising photocatalytic activity could be attributed to the effective transfer and separation of photogenerated charge carriers by adding Ru as a co-catalyst, which is due to the decreased rate of electron-hole recombination. The Ru–CdS/Hall-APTES composite with 0.5 wt % of Ru exhibits a high photocatalytic H₂ evolution rate of 932.31 μmol h⁻¹ g⁻¹ under visible light irradiation corresponding to an AQE of ~7.21% at 450 nm. This approach can be used as a basis for further studies to improve the photocatalytic activity of different nanocomposites based on modified clay minerals.

FUNDING

This work was supported by Russian Ministry of Education and Science within the framework of the state task in the field of scientific activity, topic number FSZE-2020-0007.

REFERENCES

1. S. Thakur, T. Kshetri, N. H. Kim, et al., *J. Catal.* **345**, 78 (2017).
2. J. Fang, L. Xu, Z. Zhang, et al., *ACS Appl. Mater. Interfaces* **5**, 8088 (2013).
3. M. Kimi, L. Yuliati, M. Shamsuddin, et al., *Int. J. Hydrogen Energy* **36**, 9453 (2011).
4. Q. Wang, J. Lian, Q. Ma, et al., *Catal. Today* **281**, 662 (2017).
5. P. Zhou, Z. Le, Y. Xie, et al., *J. Alloys Compd.* **692**, 170 (2017).
6. X. Xu, L. Hu, N. Gao, et al., *Adv. Funct. Mater.* **25**, 445 (2015).
7. R. Shi, H. Ye, F. Liang, et al., *Adv. Mater.* **30**, 1705941 (2018).
8. X. Yang, Z. Wang, X. Lv, et al., *J. Photochem. Photobiol. A* **329**, 175 (2016).
9. S. G. Ghugal, R. Mahalik, P. Gharde, et al., *Microporous Mesoporous Mater.* **242**, 284–293 (2017).
10. F. Vaquero, R. M. Navarro, and J. L. G. Fierro, *Appl. Catal.* **203**, 753 (2017).
11. F. Vaquero, J. G. Fierro, R. Navarro Yerga, et al., *Molecules* **21**, 401 (2016).
12. L. Ma, H. Sun, Y. Zhang, et al., *Nanotechnology* **19**, 115709 (2008).
13. D. Rawtani, Y. K. Agrawal, and D. Rawtani, *Rev. Adv. Mater. Sci.* **30**, 282 (2012).
14. M. Massaro, C. G. Colletti, G. Lazzara, et al., *J. Mater. Chem. A* **5**, 13276 (2017).
15. Y. Lvov, W. Wang, L. Zhang, et al., *Adv. Mater.* **28**, 1227 (2016).
16. A. F. Peixoto, A. C. Fernes, C. Pereira, et al., *Microporous Mesoporous Mater.* **219**, 145 (2016).
17. P. Yuan, P. Southon, Z. Liu, et al., *J. Phys. Chem. C* **112**, 15742 (2008).
18. E. Bischoff, T. Daitx, D. A. Simon, et al., *Appl. Clay Sci.* **112** (113), 68 (2015).
19. X. Wang, Y. Chen, W. Zhang, et al., *Korean J. Chem. Eng.* **33**, 3504 (2016).

20. P. Yuan, P. D. Southon, and Z. Liu, *Nanotechnology*, 375705 (2012).
21. M. Zou, M. Du, M. Zhang, et al., *Mater. Res. Bull.* **61**, 375 (2015).
22. G. Colon, *Appl. Catal. A* **518**, 48 (2016).
23. K. C. Christoforidis and P. Fornasiero, *Chem. Cat. Chem.* **9**, 1523 (2017).
24. X. Zong, H. Yan, G. Wu, et al., *J. Am. Chem. Soc.* **130**, 7176 (2008).
25. C. Kong, Z. Li, and G. Lu, *Int. J. Hydrogen Energy* **40**, 5824 (2015).
26. V. A. Vinokurov, A. V. Stavitskaya, E. V. Ivanov, et al., *ACS Sustain. Chem. Eng.* **5**, 11316 (2017).
27. F. Nekouei, S. Nekouei, and H. Kargarzadeh, *Chem. Eng. J.* **335**, 567 (2018).
28. H. Kang, X. Liu, S. Zhang, and J. Li, *RSC Adv.* **7**, 24140 (2017).
29. Z. Jin, W. Duan, W. Duan, et al., *Appl. Catal. A* **517**, 129 (2016).
30. J. Yuan, J. Wen, Q. Gao, et al., *Dalton Trans.* **44**, 1680 (2015).
31. T. Di, B. Zhu, J. Zhang, et al., *Appl. Surf. Sci.* **389**, 775 (2016).
32. H. Yu, F. Chen, F. Chen, and X. Wang, *Appl. Surf. Sci.* **358**, 385 (2015).
33. B. Han, S. Liu, N. Zhang, Y.-J. Xu, et al., *Appl. Catal. B* **202**, 298 (2017).
34. S. Ma, J. Xie, J. Wen, et al., *Appl. Surf. Sci.* **391**, 580 (2017).
35. W. Zhen, X. Ning, B. Yang, et al., *Appl. Catal. B* **221**, 243 (2018).
36. Q. Wang, J. Lian, Q. Ma, et al., *Catal. Today* **281**, 662 (2017).
37. D. You, B. Pan, F. Jiang, et al., *Appl. Surf. Sci.* **363**, 154 (2016).
38. Y. Su, D. Ao, H. Liu, and Y. Wang, *J. Mater. Chem. A* **5**, 8680 (2017).
39. H. Yu, X. Huang, P. Wang, and J. Yu, *J. Phys. Chem. C* **120**, 3722 (2016).
40. Y. Hu, X. Hao, Z. Cui, et al., *Appl. Catal. B* **260**, 118131 (2020).
41. M. Marchelek, E. Grabowska, T. Klimczuk, et al., *Appl. Surf. Sci.* **393**, 262 (2017).
42. N. Buhler, K. Meier, and J. F. Reber, *J. Phys. Chem.* **88**, 3261–3268 (1984).